# Roundness and Aspect Ratio of Particles in Ice Clouds

**ARTICLE** *in* JOURNAL OF THE ATMOSPHERIC SCIENCES · AUGUST 2003

Impact Factor: 3.14 · DOI: 10.1175/1520-0469(2003)060<1795:RAAROP>2.0.CO;2



**2 AUTHORS**, INCLUDING:

A. V. Korolev
Environment Canada
**125** PUBLICATIONS **2,791** CITATIONS

# Roundness and Aspect Ratio of Particles in Ice Clouds

ALEXEI KOROLEV

*Sky Tech Research, Inc., Richmond Hill, Ontario, Canada*

GEORGE ISAAC

*Cloud Physics Research Division, Meteorological Service of Canada, Toronto, Ontario, Canada*

(Manuscript received 3 May 2002, in final form 6 March 2003)

ABSTRACT

The frequency of occurrence of the aspect ratio and roundness of particles in ice clouds from aircraft observations have been examined. Images of cloud particles were measured by a cloud particle imager (CPI) at 2.3-$\mu$m resolution, installed on the National Research Council (NRC) of Canada Convair-580. Data were collected in winter midlatitude and polar stratiform clouds associated with frontal systems during three field projects in the Canadian and U.S. Arctic and over the Great Lakes. Approximately $10^6$ images of particles measured in ice clouds were included in the statistics. The frequency of occurrence of the aspect ratio and roundness were calculated in eight 5° temperature intervals from −40°C to 0°C. In each temperature interval, the distributions were calculated for 12 size intervals in the range from 20 $\mu$m to 1 mm. It was found that the roundness is a function of particle size and within each size interval it does not depend significantly on temperature. However, the aspect ratio of particles with 60 $\mu$m $< D <$ 1000 $\mu$m is mainly a function of temperature and does not depend on size. The fraction of spherical particles in ice clouds rapidly decreases with particle size. The fraction of spherical particles in the size range 20 $\mu$m $< D_{\max} <$ 30 $\mu$m on average does not exceed 50%. Ice clouds do not contain significant numbers of spherical particles larger than 60 $\mu$m. The information on the habits of small ice particles obtained here gives an insight on the mechanisms of ice formation in clouds. The results can be used for parameterization of particle habits in radiation transfer, weather and climate models, and in remote sensing retrievals. It may also be of interest for calculations of collision efficiency in modeling of interaction of cloud particles with moving platforms related to in-flight icing.

## 1. Introduction

The shape of an ice particle defines its scattering properties, its growth rate, and its terminal fall velocity. The scattering properties of cloud ice particles may significantly affect the climate and radiation balance of the earth (Liou and Takano 1994; Zhang et al. 1999). For climate change predictions, forecasting of precipitation and remote sensing retrievals, idealized crystal shapes such as columns, needles, plates, and dendrites are often assumed. Recent studies have shown that ''irregular'' is the dominant ice particle shape descriptor in natural clouds at temperatures ranging from 0°C down to −40°C (Korolev et al. 1999, 2000). A simple visual analysis of irregularly shaped particles shows a great variety of different forms, which cannot be covered by any of the existing classifications of cloud ice particles (e.g., Magono and Lee 1966). A description of the large variety of ice particle habits is not a simple task. Presently, there is no universal approach to the characterization of arbitrarily shaped ice particles. One application of such a future characterization should be a parameterization of particle habit that could be accommodated by numerical models predicting the radiative properties of the atmosphere, weather, and climate.

The dimensional relationships for ice particles having simple forms like plates, columns, and dendrites were studied by different authors, for example, Ono (1969), Auer and Veal (1970), Heymsfield (1972), and Hobbs et al. (1974). Later, the results of these studies were used for the parameterization of ice particle habits in radiation models (e.g., Fu 1996; Fu et al. 1999). Although some authors have attempted to treat aggregates and/or irregular-shaped ice particles, there is no physically based method for accurately determining the dimensional relationships for irregular ice particles.

In the present work, cloud particle shapes were studied with the help of a cloud particle imager (CPI) installed on the National Research Council (NRC) of Canada Convair-580. The shape of the cloud particles was described by two dimensionless parameters: aspect ratio and a defined roundness parameter. The statistics of the

*Corresponding author address:* Alexei Korolev, 28 Don Head Village Blvd., Richmond Hill, ON L4C 7M6, Canada.
E-mail: Alexei.Korolev@rogers.com

aspect ratio and roundness were calculated for different size ranges and temperature intervals.

## 2. Instrumentation

Aircraft data were collected from the National Research Council of Canada Convair-580, which was extensively equipped for cloud microphysical measurements. The images of cloud particles were recorded by a CPI probe developed by SPEC, Inc. (Boulder, Colorado), for imaging of cloud particles from high-speed moving platforms (Lawson et al. 2001). The CPI is a relatively new instrument that utilizes innovative technologies to record high-resolution digital images. A high-power pulsed laser freezes the particle image on a digital charge-coupled device (CCD) camera having $1024 \times 1024$ pixels, with a pixel resolution of 2.3 $\mu$m. A video engine processes up to 40 frames per second identifying and sizing up to 1000 particles per second. The 256-gray-level resolution provides a photographic quality images of the cloud particles.

The other cloud microphysical instrumentation relevant to this study include: a Goodrich Corporation Sensor Systems Rosemount icing detector (RICE; Mazin et al. 2001; Cober et al. 2001); two Rosemount temperature probes and a reverse-flow temperature probe; a Cambridge EG&G, Inc., dewpoint hygrometer; two Particle Measuring Systems (PMS) foreward-scattering spectrometer probes (FSSP-100; Knollenberg 1981), which measured droplet size distributions in two different size ranges of 2–32 $\mu$m and 5–95 $\mu$m; two PMS King probes (King et al. 1978); a hot-wire Nevzorov liquid water content/total water content (LWC/TWC) probe (Korolev et al. 1998); a PMS optical array probe–2DC (OAP-2DC; 25–800 $\mu$m); a PMS OAP-2DC Gray (25–1600 $\mu$m); and a PMS OAP-2DP (200–6400 $\mu$m; Knollenberg 1981). The three PMS OAP probes provided shadow images and concentration of hydrometeors within their respective size ranges. Though PMS OAP-2DC and OAP-2DP cover a wide range of particle sizes, their images could not be used in this study for the reasons discussed in section 3e.

The data described below were collected in winter midlatitude and polar clouds during three flight projects: the Third Canadian Freezing Drizzle Experiment (CFDE III) conducted in the Great Lakes Region from December 1997 to February 1998 (Isaac et al. 2001); the First International Satellite Cloud Climatology Project (ISCCP) Regional Experiment (FIRE) Arctic Cloud Experiment (ACE) conducted in the Canadian and U.S. Arctic during April 1998; and the Alliance Icing Research Project (AIRS) conducted over southern Ontario and Montreal region between November 1999 and February 2000 (Isaac et al. 2001). The temperature of the investigated clouds ranged from 0°C to −40°C. Most of the data were sampled in stratiform clouds associated with frontal systems. The altitude of the airplane during measurements varied from 0.1 to 7.5 km. The data presented in this study were collected during 44 flights. The analysis was performed only for ice clouds, with no measurable liquid water. The total number of images analyzed from these ice clouds was about 897 033 detected over a pathlength of 6513 km.

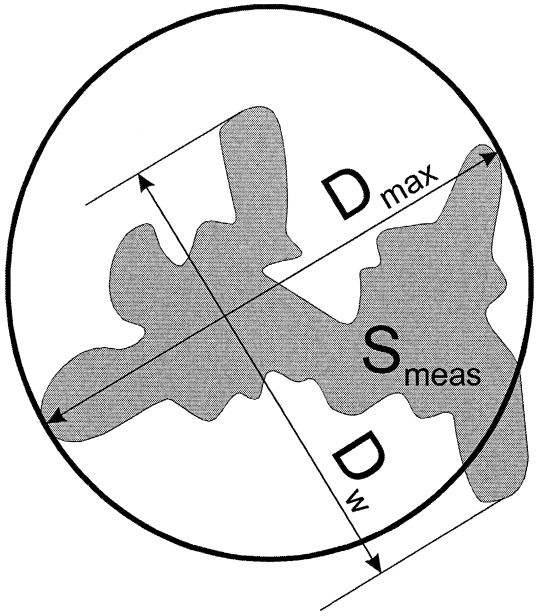


FIG. 1. Definition of $D_{max}$ and $D_w$ used in the present study to analyze cloud particle shapes.

## 3. Data processing and accuracy of measurements

### a. Image processing

The habit of the particles in the present study was characterized by two dimensionless parameters. First,

$$\alpha = \frac{D_w}{D_{\max}}, \tag{1}$$

and second,

$$\beta = \frac{4S_{\text{meas}}}{\pi D_{\max}^2}, \tag{2}$$

where $S_{\text{meas}}$ is the measured projection area of the particle image, $D_{\max}$ is the maximum dimension of the image, and $D_w$ is the maximum dimension of the image in the direction perpendicular to $D_{\max}$ (Fig. 1). In the following discussion $D_{\max}$ will be referred to as ''length'' and $D_w$ as ''width'' of the image. Both parameters $\alpha$ and $\beta$ vary from 0 to 1; $\alpha$ represents an aspect ratio of the image, while $\beta$ characterizes an area density of the image (Fig. 1). If $\alpha = 1$ the image may have a shape quite different from a circle (Fig. 1). As $\beta$ approaches 1, the image becomes closer to a circle. Therefore, the parameter $\beta$ can be considered a measure of the circularity or ''roundness'' of the particle images. It was assumed here that a circular shape implies a spherical

particle. In the following discussion, $\alpha$ and $\beta$ will be referred to as ''aspect ratio'' and roundness, respectively. The parameters $S_{\text{meas}}$, $D_{\max}$, and $D_w$ were extracted from raw CPI data by the CPIVIEW software developed by SPEC, Inc.

### b. Segregation of ice clouds

To eliminate the effect of liquid droplets on the statistics of ice particle habits, the CPI data were analyzed only for ice clouds. The clouds were considered ''ice clouds'' if at least one of the following two conditions was satisfied (Korolev et al. 2003):

$$\frac{W_{\text{ice}}}{W_{\text{ice}} + W_{\text{liquid}}} > 0.9, \tag{3}$$

$$dV_{\text{RICE}}/dt \leq 0, \tag{4}$$

where $W_{\text{ice}}$ and $W_{\text{liquid}}$ are the ice and liquid water content, respectively; $V_{\text{RICE}}$ is the ramp voltage of the RICE. The $W_{\text{ice}}$ and $W_{\text{liquid}}$ were extracted from the Nevzorov probe measurements as described in Korolev et al. (2003). Condition (3) implies that an ice cloud may still contain up to 10% of liquid water. The ratio in condition (3) was set to 0.9 due to the uncertainty in the response of the Nevzorov LWC sensor to ice. The residual effect of ice on the LWC sensor is due to the small amount of heat removed from the LWC sensor during collision with ice particles. The residual effect depends on size, shape and bulk density of ice particles, air speed, air temperature, and the temperature of the sensor (Korolev et al. 1998; Strapp et al. 1999). It was found that the residual effect of ice on the LWC sensor is, on average, 11% of the measured TWC in ice clouds at 100 m $s^{-1}$ (Korolev et al. 2003), which is close to the speed of the Convair-580.

In some ice clouds the residual effect may exceed 11%. To include these cases in the data analysis condition (4) was used. Condition (4) considers cases when the RICE signal either decreases due to evaporation of ice (Mazin et al. 2001) or stays constant. The evaporation of ice occurs due to adiabatic heating on the surface of the RICE detector. The threshold sensitivity of the RICE detector due to the adiabatic heating effect was estimated as about 0.006 g $m^{-3}$ at 100 m $s^{-1}$ (Mazin et al. 2001). This value agrees with threshold sensitivity 0.007–0.01 g $m^{-3}$ found experimentally by Cober et al. (2001) for the RICE installed on the NRC Convair-580.

The two ''phase separation'' methods associated with conditions (3) and (4) are complimentary and they provide accurate segregation of ice clouds. The deicing cycle of the RICE probe may vary from 5 to 15 s. During this period of time the RICE does not provide adequate measurements, and the glaciated zones embedded in the mixed-phase clouds may be missed. At the same time, the Nevozorov probe provides continuous measurements, which allows gaps to be filled in the RICE probe measurements.

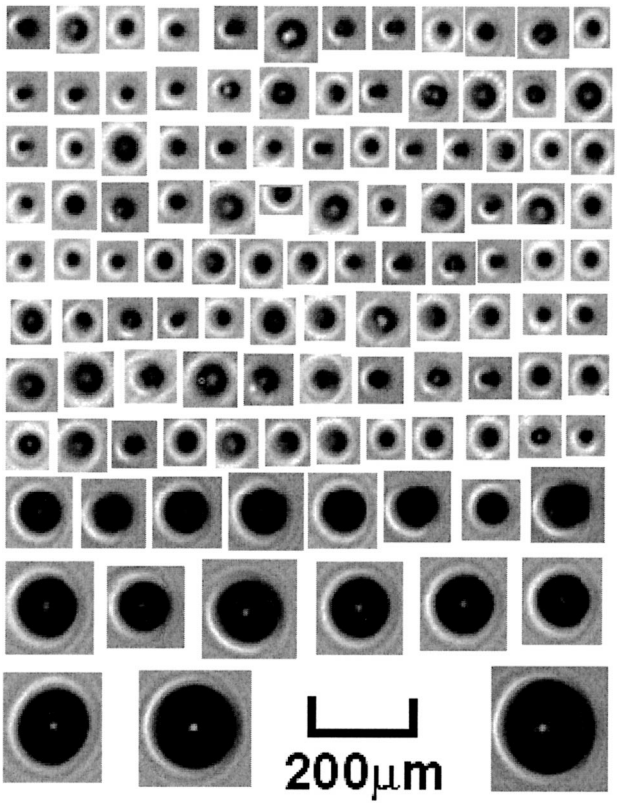


FIG. 2. Images of liquid droplets measured by the CPI in a liquid stratocumulus. Lake Ontario, 2216:35–2217:30 UTC 18 Feb 2000, $T = -5$°C, $H = 3000$ m.

It follows that conditions (3) and (4) allow the presence of small amounts of liquid water in clouds defined as ice clouds. This is related to the accuracy of the instruments used for the segregation of ice and liquid phase in clouds.

### c. Sensitivity of images to distortion effects

Distortion of the cloud particle images by probes like the CPI occurs due to digitizing and optical aberrations. The effect of the distortion factors was tested using cloud droplets having a known spherical shape. Figure 2 shows an example of cloud droplets measured by the CPI in a liquid cloud containing drizzle. The cloud was estimated as ''liquid'' since LWC≈TWC and no ice particles were detected by OAP-2D probes and CPI. Due to optical aberrations, some images of droplets may be distorted and, thus, deviate from a circle. A small fraction of the images viewed by the CPI are partials. An example of such an image is shown in the fourth row in Fig. 2. Partial images also result in noncircular shapes for spherical particles. The effect of such distorting factors can be estimated from Fig. 3, which shows the frequency distributions of roundness and aspect ratio for the liquid cloud of Fig. 2. For ideal images of spheres, both the roundness and aspect ratio should be

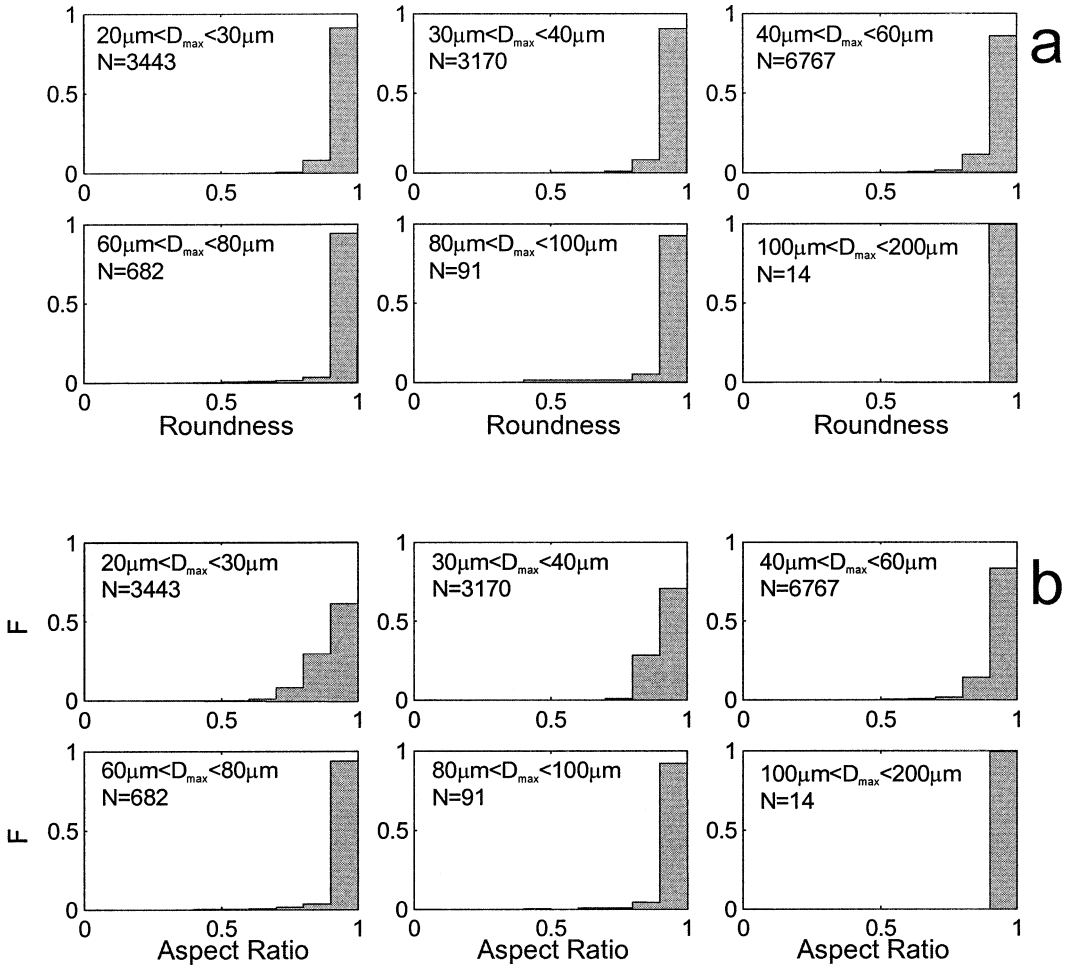


FIG. 3. Distribution of (a) roundness and (b) aspect ratio calculated for liquid droplets measured in an all-liquid cloud. Images of these droplets are shown in Fig. 2. The numbers in the upper left corners indicate the size range and the number of particles in the sample. Lake Ontario, Sc, 2216:12–2305:30 UTC 18 Feb 2000, $T = -5$°C, $H = 3000$ m.

equal to one. As seen from Fig. 3a, for about 90% of all cases for droplets with 20 $\mu$m $< D <$ 200 $\mu$m and roundness $\beta > 0.9$. Figure 3b shows that the aspect ratio of the CPI images of spherical particles decreases with droplet size. For droplets with 20 $\mu$m $< D <$ 30 $\mu$m, only about 60% of the images have an aspect ratio $\alpha > 0.9$. Therefore, the aspect ratio of the CPI images is more sensitive to distortion factors in comparison to the roundness parameter.

### *d. Imaging of ice particles*

The evaluation of the image quality of small ice particles was conducted for particles sampled in ice clouds, which were selected in accordance with conditions (3) and (4). Figure 4 shows variations of altitude, temperature, RICE ramp voltage, LWC, and TWC along the flight of the Convair-580 on 16 February. As seen from Fig. 4, the measurements were conducted during the ascent of the plane through two cloud layers. The lower cloud layer (from 1139:40 to 1141:00 UTC) was liquid because LWC≈TWC. The upper layer (from approximately 1142:40 to 1145:40 UTC) was defined as ice clouds due to condition (4). Condition (3) was not met in the ice cloud because $W_{\text{ice}}/(W_{\text{ice}} + W_{\text{liquid}}) < 0.9$. However, ice that accumulated on the surface of the RICE probe near 1140 UTC was gradually sublimating after this time. The rate of ice sublimation near 1144 UTC calculated for the RICE calibrating coefficient $k = 1.4 \times 10^{-5} \pm 0.14 \times 10^{-5}$ kg V$^{-1}$ (Mazin et al. 2001) was close to $4.3 \times 10^{-8} \pm 0.3 \times 10^{-8}$ kg s$^{-1}$. The rate of sublimation is a function of temperature, pressure, air speed, and humidity. Following the method developed by Mazin et al. (2001) the obtained rate of ice sublimation would correspond to 75% humidity at $T = -30$°C, $P = 470$ mb, and true air speed (TAS) = 120 km h$^{-1}$. Such humidity at $-30$°C is close to the saturation water vapor pressure over ice. Under these conditions liquid droplets either freeze or quickly evaporate. Therefore, the ice cloud (1142:40 to 1145:40

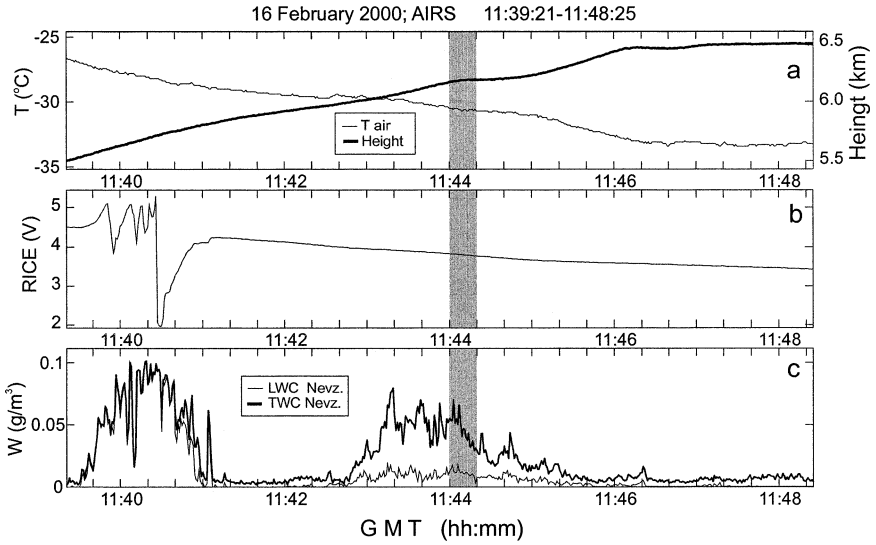


FIG. 4. Time history of (a) latitude and temperature, (b) ramp voltage of the RICE probe, and (c) LWC and TWC derived from the Nevzorov probe along the flight of the NRC Convair-580 on 1139:21–1148:25 UTC 16 Feb 2000.

UTC) does not contain liquid droplets. The liquid water $W_{\text{liquid}} \approx 0.01$ g m$^{-3}$ derived from the Nevzorov probe measurements is likely caused by the residual effect of ice.

Figure 5 shows cloud particles registered by the CPI during the time period 1144 to 1145 UTC as indicated by the gray band in Fig. 4. As seen from the top part of Fig. 5a, a large fraction of the ice particles yields circular images similar to those in Fig. 2, which resulted from liquid droplets. Larger particles develop more features and deviate from circularity.

### *e. Accuracy of roundness and aspect ratio*

For ideal optics, the accuracy of the measurement of roundness and aspect ratio depend on the ratio of the particle size to the pixel resolution. The larger this ratio, the better the digital image reproduces the actual one, and thus the calculation of $\alpha$ and $\beta$ is more accurate. The length of the smallest particle considered in the present study is 20 $\mu$m, which corresponds to eight pixels at 2.3-$\mu$m resolution. A random error in digitizing an image is usually one pixel. Therefore, for an eight-pixel-wide circular image, the error in the aspect ratio may reach 23%. This error explains why the counts of the aspect ratio for 20 $\mu$m $< D <$ 30 $\mu$m droplets are distributed over three bins in Fig. 3b. For the size bins 30 $\mu$m $< D <$ 40 $\mu$m and 40 $\mu$m $< D <$ 60 $\mu$m the relative errors in the aspect ratio are about 13% and 8%, respectively. It should be noted that, for the size range 20 $\mu$m $< D <$ 30 $\mu$m, a particle with an aspect ratio less than 0.12 cannot be resolved. Optical aberrations in the CPI and errors associated with the depth of field would move this threshold to approximately 0.3. However, the distributions shown in Fig. 7 (below) indicate that the particles with $\alpha < 0.5$ do not exist in significant numbers in the size range 20 $\mu$m $< D <$ 30 $\mu$m.

The estimation of the digitizing errors on roundness is more complex. Figure 6 demonstrates an effect of digitizing for the same image sampled with different pixel resolution. The image in Fig. 6a is 123 pixels in length, and the same image sampled at a lower resolution in Fig. 6b has 15 pixels. The roundness for the high- and low-resolution images shown in Figs. 6a and 6b are 0.69 and 0.73, respectively. This corresponds to a 6% error. The errors in roundness in addition to digitizing, depend on the particle shape. The largest errors in roundness are associated with the smallest size range 20 $\mu$m $< D <$ 30 $\mu$m. However, the roundness of spherical particles with 20 $\mu$m $< D <$ 30 $\mu$m is reproduced with relatively small errors of about 10% (Fig. 3a).

Based on the above, it can be concluded that the errors in the roundness and aspect ratio due to digitizing can be neglected for particles larger than 15 pixels in size, or approximately 35 $\mu$m in diameter.

The main source of errors affecting the roundness and aspect ratio is associated with optical aberrations and out-of-focus images. When a particle moves out of the object plane, it becomes more blurred and the intensity of the image increases (Korolev et al. 1998). Therefore, the intensity level of the image may be used as a criterion to reject out-of-focus images. The settings for the image analysis during the processing were adjusted to reduce the errors related to the depth-of-field issue. After a number of experiments it was found that the settings in the CPIVIEW software—median filter order 2, region of interest (ROI) darkness threshold $-40$, and gradient threshold 100—give the best compromise between the number of accepted images and its quality. These settings reject out-of-focus images and leave sharp ones.

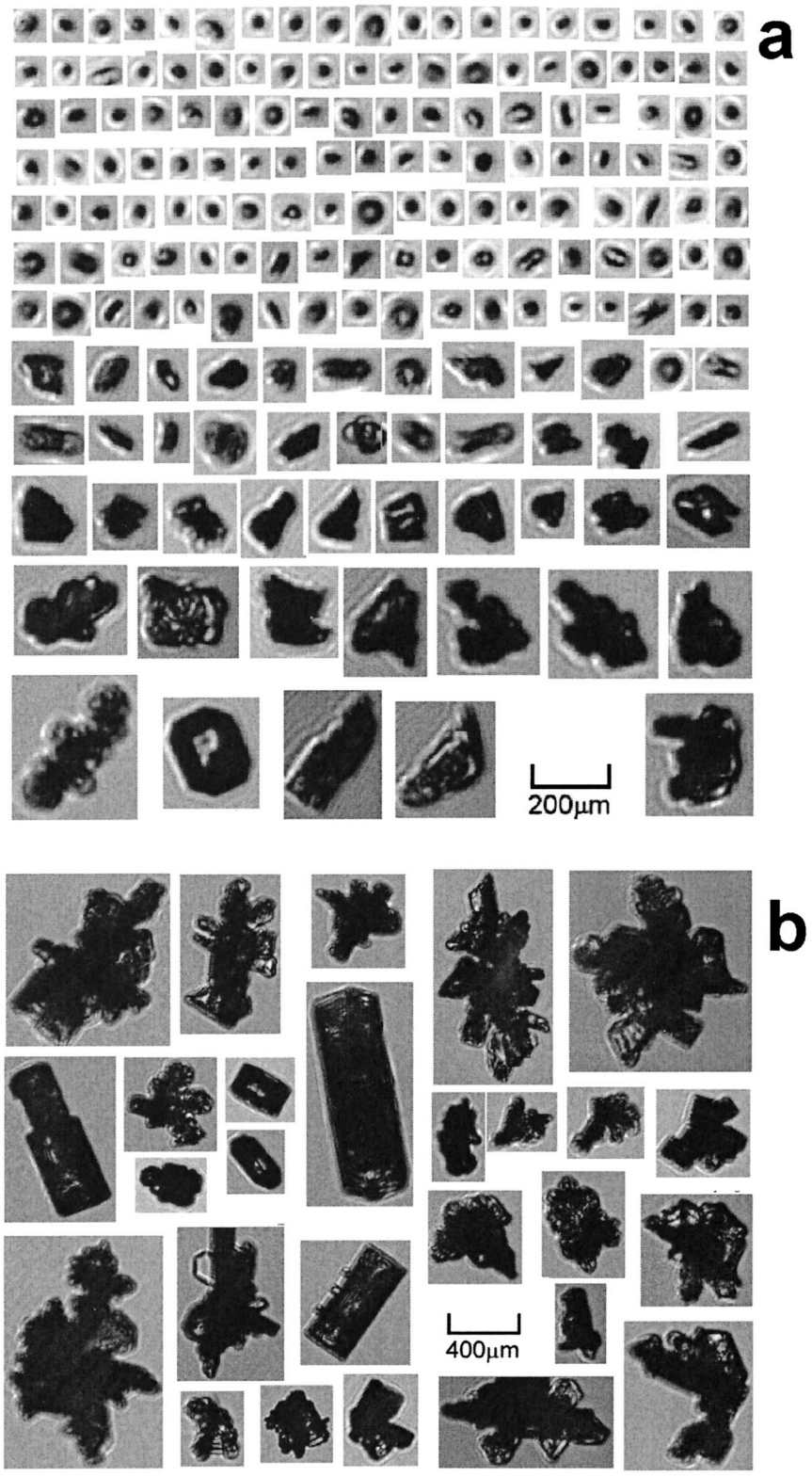


FIG. 5. Images of cloud particles measured in an ice cloud within the time interval indicated by gray shade in Fig. 4. Small particles in (a) have a lot of circular images.

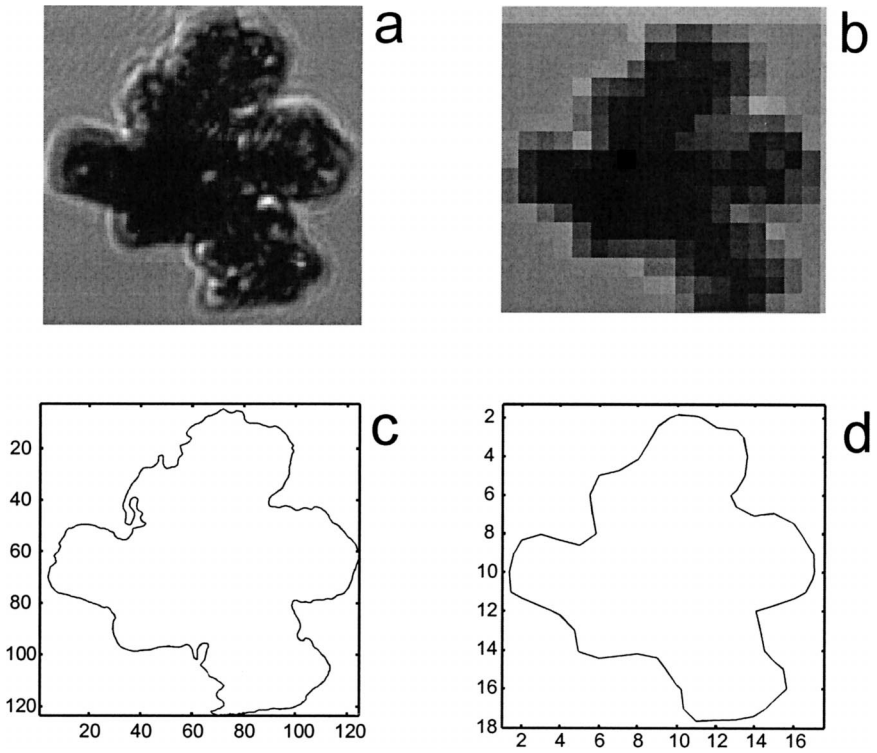


FIG. 6. Two identical images sampled at (a) high and (b) low pixel resolution. (c), (d) Diagrams show corresponding perimeters of the high- and low-resolution images, respectively.

Errors related to the CPI optical aberrations eluded analysis. It should be noted that the errors depend on the quality of the optics, optical alignment, and contamination of the optics. Analysis of individual images showed that for the CPI used in the present study, the errors in $\alpha$ and $\beta$ can be neglected for particles larger 60 $\mu$m.

The use of the OAP-2DC and OAP-2DP probes for calculation of the roundness and the aspect ratio is plagued by low pixel resolution. As discussed above, for calculations of the roundness, the image should be at least eight pixels wide. Therefore, the OAP-2DC and OAP-2DP probes at 25-$\mu$m and 200-$\mu$m pixel resolution and 32-element diode array can cover the size ranges 200 to 750 $\mu$m and 1600 to 6000 $\mu$m, respectively, for the calculations of roundness. Note, that the gap from 750 to 1600 $\mu$m is not covered by the OAP-2DC and OAP-2DP probes. Beside this, the OAP images may have different resolutions in the $X$ and $Y$ directions due to errors in adjusting the frequency of scanning the photodiode array. As a result, the calculated aspect ratio and roundness would be biased.

## 4. Results

### *a. Roundness*

Figure 7 shows the frequency distributions of roundness in eight 5°C temperature intervals from $-40°$ to 0°C. In each temperature interval, the distributions were calculated for 12 size intervals (as noted in the upper left of each histogram) in the range from 20 $\mu$m to 2 mm. The probability ($F$) of finding each value of roundness between 0 and 1 is given for each histogram. The number ($N$) of crystals analyzed for each histogram is also given just below the designated size interval.

The comparisons of the size distribution measured by the CPI and that measured by conventional cloud particle spectrometers (PMS FSSPs, OAPs) showed that the CPI probe samples particles in a biased manner. The magnitude of the bias for large particles ($D > 80$ $\mu$m) depends on the particle detecting system (PDS) threshold and other CPI settings used during measurements. For small particles ($D < 80$ $\mu$m), besides the above settings, it also depends of depth-of-field problems. For this reason the frequency of occurrence of the roundness and aspect ratio were considered for relatively narrow size bins. The only assumption behind this is that the effect of distortion factors is the same for particles within the same size bin. In other words, the size distribution in each size bin was considered uniform. This is a standard assumption used in all cloud particle size spectrometers. Therefore, the effect of biased particle sampling was minimized and in general does not affect the results presented in the following sections.

It can be concluded from Fig. 7 that the modal value of the roundness stays approximately the same in each

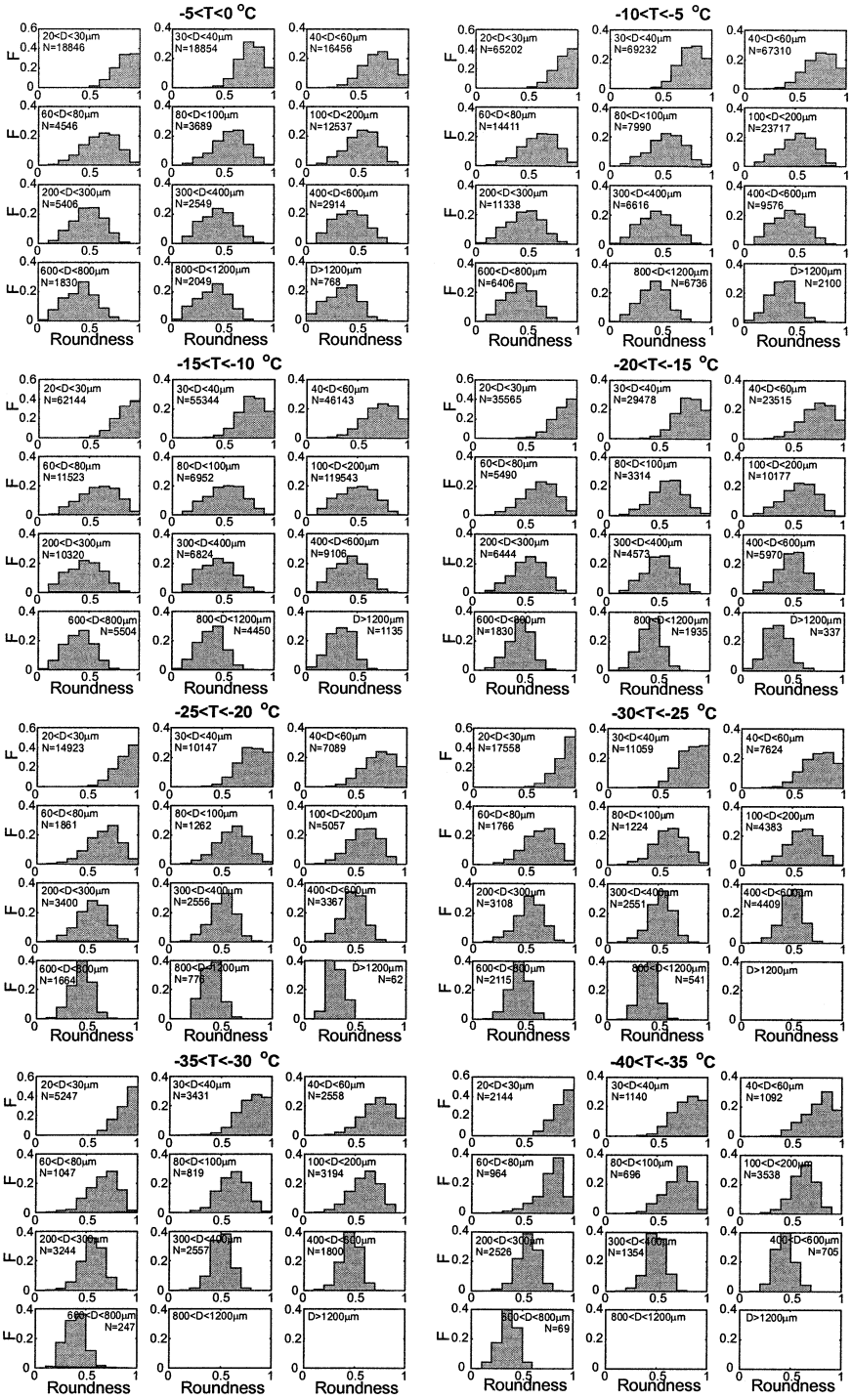


FIG. 7. Distributions of roundness in different size ranges and temperature intervals calculated for images of cloud particles measured by the CPI in ice clouds. Numbers in the top-left corners indicate the size ranges and the sample statistics for each distribution.

size range for all temperature intervals. The width of the roundness frequency distributions decreases toward cold temperatures; that is, the roundness distribution becomes narrower with a decrease of temperature.

Figure 8 shows the mean and median roundness versus particle size for different temperature intervals. In each temperature interval the average roundness rapidly decreases from 0.9 to 0.6, when the size changes from 20 to 80 $\mu$m (Fig. 8). At sizes larger than 80 $\mu$m, there is a slow decrease of the average roundness to about

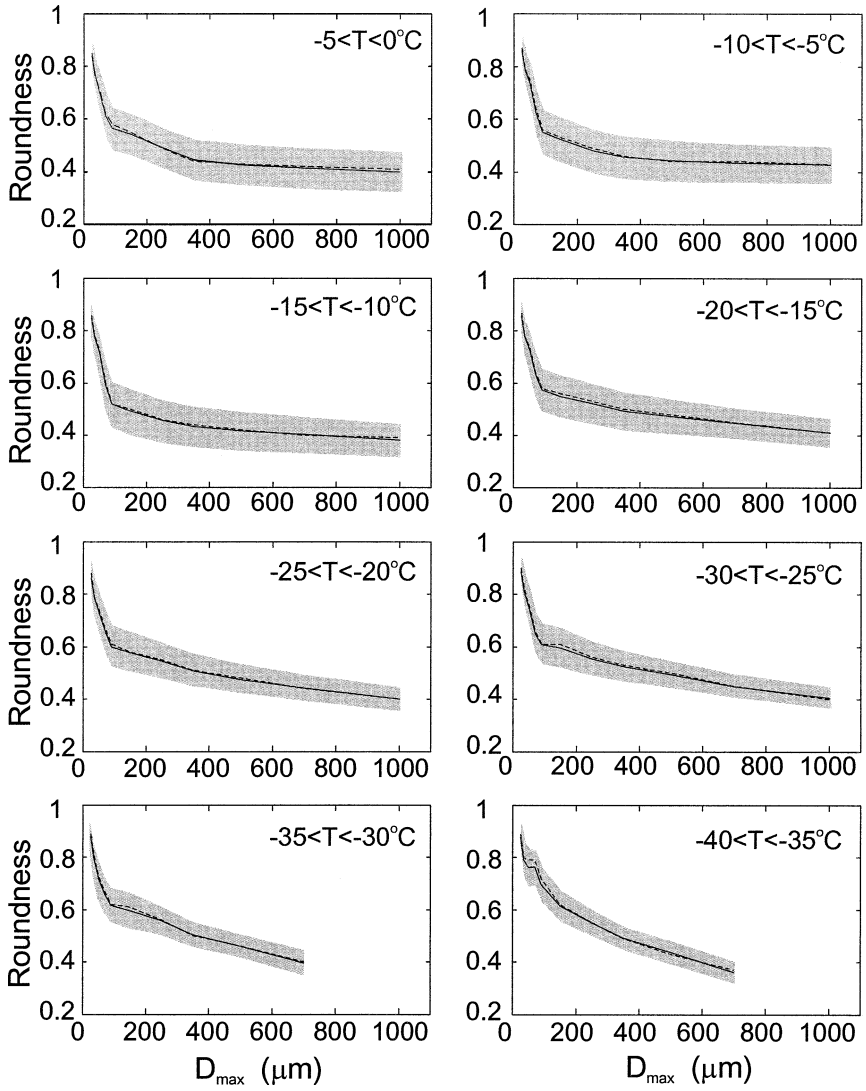


FIG. 8. Mean (solid) and median (dashed) roundness of particles in ice clouds vs particle length. The gray band indicates the std dev.

0.4. It should be noted that the rate of decrease of the average roundness at sizes larger than 80 $\mu$m increases with colder temperatures, and it has a maximum at $-40°C < T < 35°C$. In the temperature interval $-10°C < T < -0°C$, the roundness of particles larger than 350 $\mu$m stays nearly constant and equal to about 0.4–0.45.

Figure 9 presents the same dataset from a different perspective. It shows roundness versus temperature for different image sizes. The most striking feature of Fig. 9 is that the roundness of particles is a weak function of temperature and it stays approximately constant in each size interval.

The independence of the roundness on temperature is an interesting phenomenon. Early laboratory experiments revealed that the rate of propagation of the basal faces (along the *c* axis), relative to that of prism faces (along the *a* axis) varies with temperature and supersaturation in a characteristic manner (e.g., Nakaya 1954; Kobayashi 1957; Hallett and Mason 1958; Rottner and Vali 1974). Therefore, one would expect to observe certain types of ice particle habits in clouds at certain temperatures. Observation of ice particle shapes in natural conditions collected by different authors have been summarized by Magono and Lee (1966) in the well-known Magono–Lee diagram. However, recent analysis of ice particle habits from in situ measurements have suggested that irregular is the dominant form of ice particles grown in natural clouds in all temperature intervals (Korolev et al. 1999, 2000). The obtained results indicate that the roundness of these irregular particles is a function of size but not the temperature. A particle of the same size would have, on average, the same roundness in all temperature intervals. This may have a big impact on radiative properties of ice clouds.

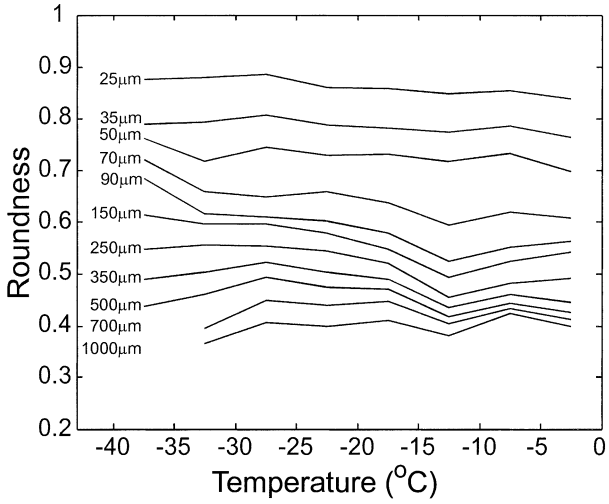


FIG. 9. Mean roundness vs temperature for different size ranges. Std dev is available from Fig. 8.

*b. Aspect ratio*

Figure 10 shows the frequency distributions of aspect ratio in different size ranges and temperature intervals. The distributions of the aspect ratio for $D_{max} > 300$ $\mu$m stay approximately the same at temperatures $-25°C < T < 0°C$. Similar to the roundness there is a tendency of the aspect ratio distribution to get narrower toward colder temperatures.

Figure 11 shows the mean and median aspect ratio versus image length for different temperature intervals. It was interesting to find that, at temperatures $-30°C < T < 0°C$, the average aspect ratio for 20 $\mu$m $< D_{max} <$ 80 $\mu$m rapidly decreases from about 0.8 to 0.6 and then, for $D_{max} > 80$ $\mu$m, it stays approximately constant.

Figure 12 presents aspect ratio versus temperature for different image sizes. The aspect ratio of small particles (20 $\mu$m $< D_{max} <$ 60 $\mu$m) was found to stay approximately constant with temperature. The aspect ratio of particles with $D_{max} > 60$ $\mu$m decrease with an increase of temperature at the same rate, independent of particle size.

*c. Fraction of spherical particles in ice clouds*

The distributions of the roundness and aspect ratio shown in Fig. 3 can be considered as distortion functions and therefore be used for retrievals of the fraction of spherical images in measured distributions. For example, if the distribution of the aspect ratio for spherical particles only results in 60% counts in the bin $0.9 < \alpha < 1$ (Fig. 3b), then the measured distribution, having 20% counts in the same bin, shows 33% of the particles are spherical. Figure 13 shows the fraction of circular images versus temperature for three size intervals 20 $\mu$m $< D_{max} <$ 30 $\mu$m, 30 $\mu$m $< D_{max} <$ 40 $\mu$m, and 40 $\mu$m $< D_{max} <$ 60 $\mu$m retrieved from the appropriate distributions shown in Figs. 7 and 10. As seen from Fig. 13 the fraction of circular images tends to decrease toward warm temperatures. On the other hand, the fraction of circular images rapidly decreases with an increase of particle size. Particles with $D_{max} > 60$ $\mu$m do not have circular images in significant numbers. This also can be seen from distributions shown in Figs. 7 and 10.

Considering both spherical and nonspherical particles may result in circular images (Korolev and Sussman 2000), the actual fraction of the spherical particles may be less than that shown in Fig. 13. Therefore, the diagrams shown in Fig. 13 should be considered as an upper limit of the fraction of spherical particles in ice clouds.

Many parameterizations consider small ice particles spheres. Thus, Brown and Francis (1995), in their parameterization of size to mass conversion, considered particles with $D < 100$ $\mu$m spherical ice. Fu (1996) treated ice particles smaller than 30 $\mu$m as hexagonal columns with an aspect ratio equal to one in the radiation calculations. The present study shows that only about half of the small ice particles (20 $\mu$m $< D_{max} <$ 30 $\mu$m) may have an aspect ratio close to one and be treated as spheres.

## 5. Discussion

*a. Spherical particles in ice clouds*

As was shown in section 4c, the fraction of spherical particles with 20 $\mu$m $< D <$ 30 $\mu$m in midlatitude and polar stratiform ice clouds varies from 30% to 50% depending on temperature. Stith et al. (2002) also found a large fraction of small quasi-spherical ice particles at cold temperatures in extratropical convective clouds. Are those spherical particles solid or liquid? Although we present evidence that the clouds observed in this study were glaciated, some uncertainty remains. Consequently, this question cannot be unambiguously answered at this stage of development of aircraft instrumentation because there are no probes that discriminate between small spherical ice and liquid droplets. Korolev and Isaac (2003) discussed that activation of liquid droplets might occur in small-scale (10–100 m) updrafts having a turbulent nature. These droplets may stay in a liquid condition for some time before freezing or evaporation due to the Wegener–Bergeron–Findeisen mechanism. After droplet freezing, the newly formed ice crystal would keep its spherical shape for some period of time. This time depends on supersaturation and temperature.

*b. Ice nucleation in natural clouds*

A study of the shape of small ice particles gives a clue to understanding ice nucleation, one of the fundamental questions in cloud physics. The presence of a large number of small spherical particles in almost all ice clouds (Figs. 7, 10, and 13) suggested that ice formation occurs through freezing of liquid droplets. Spherical particles are observed in large numbers even in clouds undersaturated with respect to water (Figs. 4 and 5). If ice nucleation occurs primarily on sublimation

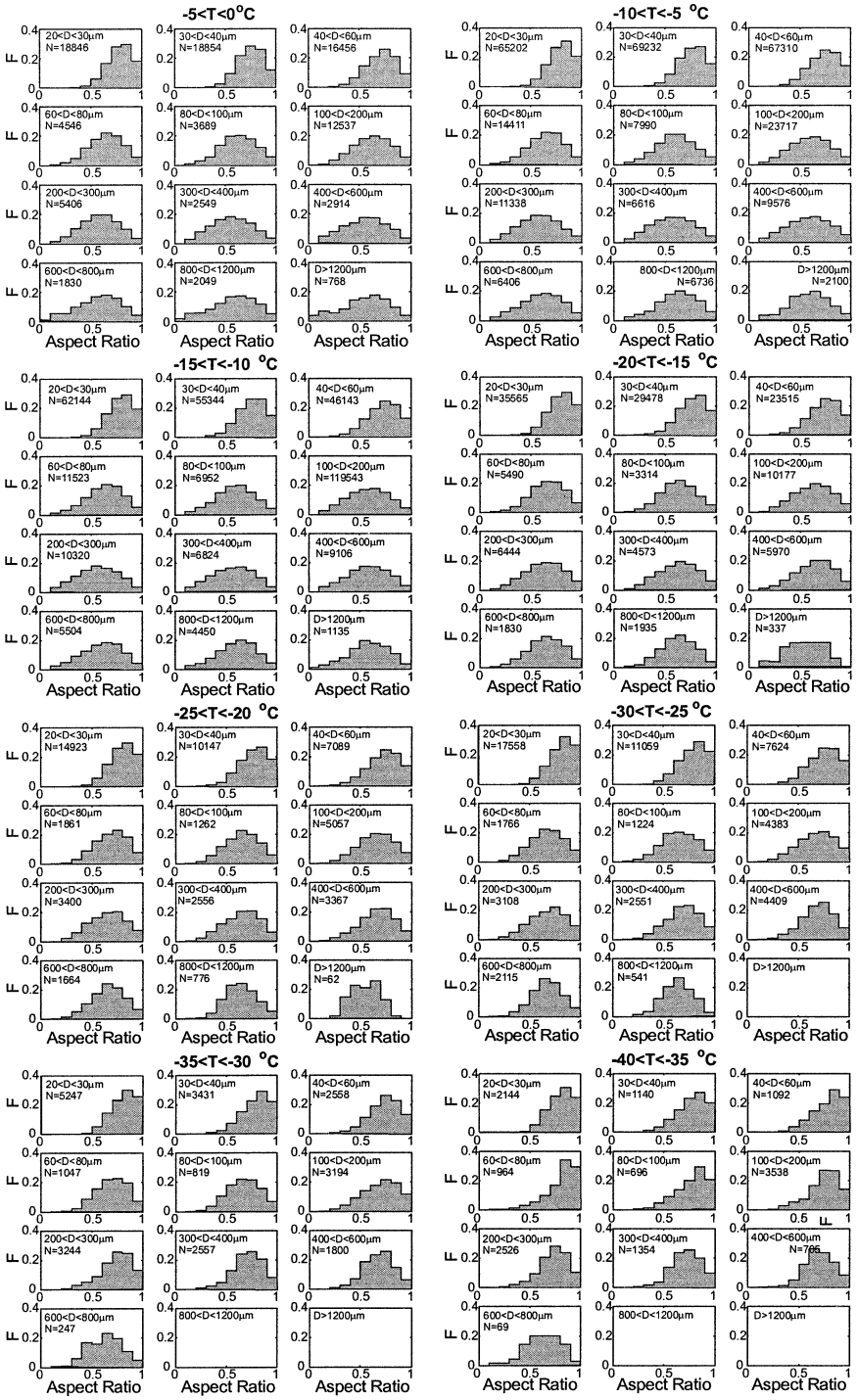


FIG. 10. Distributions of aspect ratio in different size ranges and temperature intervals calculated for images of cloud particles measured by the CPI in ice clouds.

or deposition ice nuclei, then in order to explain the large fraction of circular images in ice clouds, spherical growth of small (10–20 $\mu$m) ice particles must occur. Such growth is not observed in laboratory conditions (e.g., Gonda and Yamazaki 1984).

### *c. Habits of small ice*

One of the interesting findings is that most ice particles in the range 20 to 60 $\mu$m have significant aspect ratios (Fig. 10) and are mostly irregular in shape (Fig.

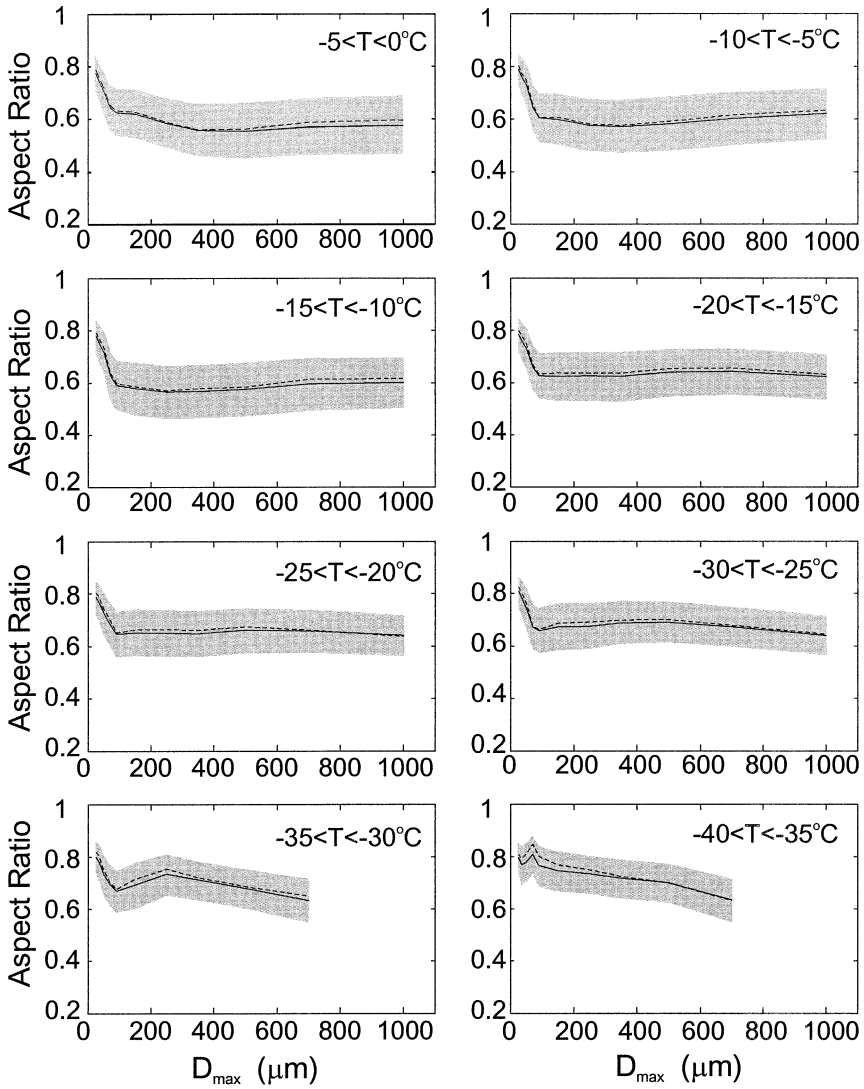


FIG. 11. Mean (solid) and median (dashed) aspect ratio of particles in ice clouds vs particle length. The gray band indicates the std dev.

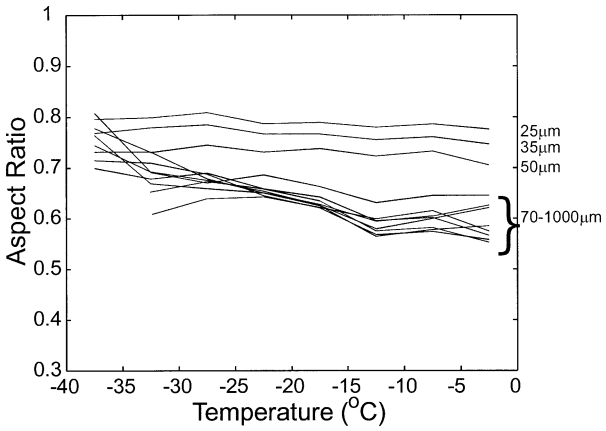


FIG. 12. Mean aspect ratio vs temperature for different size ranges. Std dev is available from Fig. 11.

5). These ice particles keep the irregular shape as they get larger, with the aspect ratio remaining relatively constant for sizes between 60 and 1000 $\mu$m, while the roundness decreases with increasing size. Only a few ice particles keep growing as pristine (Fig. 5). This is in agreement with previous studies showing that only a small fraction of ice can be classified as pristine ice, whereas the majority of ice particles fall into an irregular category (Korolev et al. 1999, 2000).

### *d. The effect of the viewing angle*

Ice particles with Reynolds number Re $>$ 10 fall with their largest cross section plane oriented horizontally (List and Shemenauer 1971). From laboratory studies, columns fall with their *c* axis horizontal, while for plates and dendrites, the *c* axis is vertical. Therefore, it is

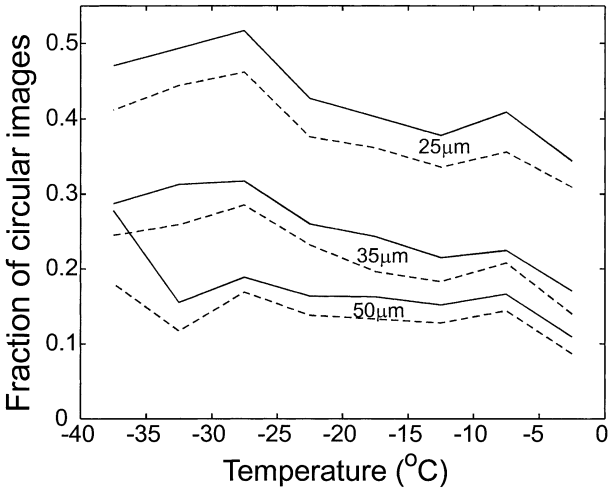


FIG. 13. Fraction of particles in ice clouds yielding circular images vs temperature derived from data on roundness (solid line) and aspect ratio (dashed line).

expected that the roundness and aspect ratio of the particle images would be a function of the viewing angle. For example, a hexagonal plate viewed from the top has an aspect ratio 0.87. However, when a plate is viewed from the side, the aspect ratio, depending on its thickness, may vary from 1 to about 0.01.

The CPI imaging laser beam has an inclination 45° to the horizon. The natural orientation of ice particles inside the CPI sampling tube is changed due to shear and the air deceleration. The effect of shear on the orientation inside the CPI sampling tube is not clear and requires a special study. Changing the orientation would not affect the statistics of $\alpha$ and $\beta$ for particles smaller than 50 $\mu$m because, for these particles, Re $< 1$ and their spatial orientation may be considered random. For particles larger than 100 $\mu$m, the disorientation of particles inside the CPI sample tube may cause a systematic bias of $\alpha$ and $\beta$ statistics.

## 6. Conclusions

The following results have been obtained.

1) The average and median roundness stay relatively constant with changes of temperature in each size bin.
2) The roundness of particles decreases with increasing size going from approximately 0.85 near 25 $\mu$m to 0.4 near 1000 $\mu$m.
3) The fraction of particles yielding circular images rapidly decreases with increasing particle size. The fraction of spherical particles in the size range 20 $\mu$m $< D_{\max} <$ 30 $\mu$m in ice clouds on average does not exceed 50%. Generally, ice clouds do not contain significant quantities of spherical particles larger than 60 $\mu$m.
4) The average aspect ratio of cloud particles changes from 0.8 to 0.6 in the temperature range $-40°\text{C} < T < 0°\text{C}$. For particles with 60 $\mu$m $< D_{\max} <$ 1000 $\mu$m the aspect ratio does not depend significantly on particle size and it mainly depends on temperature.

The information about the habits of small ice particles obtained here gives an insight into the mechanisms of ice formation in clouds. The results can be used for parameterization of particle habits in radiation transfer, weather and climate models, and in remote sensing retrievals. Data presented here may also be of interest for calculations of collision efficiency in modeling of interaction of cloud particles with moving platforms related to in-flight icing.

*Acknowledgments.* Support for the collection of the FIRE ACE data was given by MSC, NRC, the Canadian Panel on Energy Research and Development, and NASA Langley. The National Search and Rescue Secretariat of Canada, Boeing Commercial Airplane Group, Transport Canada, the Canadian Department of National Defense, NASA Glenn, and the FAA have provided funding for the CFDE and AIRS projects. The aircraft data were obtained using the National Research Council of Canada Convair-580 and the scientific and technical efforts of many NRC and MSC staff. Alexei Korolev performed this work under Contract KM175-012030/001/TOR to the Meteorological Service of Canada.

## REFERENCES

Auer, A. H., Jr., and D. L. Veal, 1970: The dimension of ice crystals in natural clouds. *J. Atmos. Sci.,* **27,** 919–926.

Brown, P. R. A., and P. N. Francis, 1995: Improved measurements of the ice water content in cirrus using a total-water probe. *J. Atmos. Oceanic Technol.,* **12,** 410–414.

Cober, S. G., G. A. Isaac, and A. V. Korolev, 2001: Assessing the Rosemount Icing Detector with in situ measurements. *J. Atmos. Oceanic Technol.,* **18,** 515–528.

Fu, Q., 1996: An accurate parameterization of the solar radiative properties of cirrus clouds for climate models. *J. Climate,* **9,** 2058–2082.

——, W. B. Sun, and P. Yang, 1999: Modeling of scattering and absorption by nonspherical cirrus ice particles at thermal infrared wavelengths. *J. Atmos. Sci.,* **56,** 2937–2947.

Gonda, and T. Yamazaki, 1984: Initial growth forms of snow ice crystals growing from frozen cloud droplets. *J. Meteor. Soc. Japan,* **62,** 190–192.

Hallett, J., and B. J. Mason, 1958: The influence of temperature and supersaturation on the habit of ice crystals grown from the vapor. *Proc. Roy. Soc. London,* **A247,** 440–453.

Heymsfield, A., 1972: Ice crystal terminal velocities. *J. Atmos. Sci.,* **29,** 1348–1357.

Hobbs, P. V., S. Chang, and J. D. Locatelli, 1974: The dimensions and aggregation of ice crystals in natural clouds. *J. Geophys. Res.,* **79,** 2199–2206.

Isaac, G. A., S. G. Cober, J. W. Strapp, A. V. Korolev, A. Tremblay, and D. L. Marcotte, 2001: Recent Canadian research on aircraft in-flight icing. *Can. Aeronaut. Space J.,* **47,** 213–221.

King, W. D., D. A. Parkin, and R. J. Handsworth, 1968: A hot-wire water device having fully calculable response characteristics. *J. Appl. Meteor.,* **17,** 1809–1813.

Knollenberg, R. G., 1981: Techniques for probing cloud microstruc-

ture. *Clouds, Their Formation, Optical Properties, and Effects*, P. V. Hobbs and A. Deepak, Eds., Academic Press, 15–91.

Kobayashi, T., 1957: Experimental researches on the snow crystal habit and growth by means of a diffusion cloud chamber. *J. Meteor. Soc. Japan 75th Anniversary Vol.*, 38–44.

Korolev, A. V., and B. Sussman, 2000: A technique for habit classification of cloud particles. *J. Atmos. Oceanic Technol.*, **17,** 1048–1057.

——, and G. A. Isaac, 2003: Phase transformation of mixed-phase clouds. *Quart. J. Roy. Meteor. Soc.*, **129,** 19–38.

——, J. W. Strapp, G. A. Isaac, and A. N. Nevzorov, 1998: The Nevzorov airborne hot-wire LWC–TWC probe: Principle of operation and performance characteristics. *J. Atmos. Oceanic Technol.*, **15,** 1495–1510.

——, G. A. Isaac, and J. Hallett, 1999: Ice particle habits in Arctic clouds. *Geophys. Res. Lett.*, **26,** 1299–1302.

——, ——, and ——, 2000: Ice particle habits in stratiform clouds. *Quart. J. Roy. Meteor. Soc.*, **126,** 2873–2902.

——, ——, S. G. Cober, J. W. Strapp, and J. Hallett, 2003: Microphysical characterization of mixed-phase clouds. *Quart. J. Roy. Meteor. Soc.*, **129,** 39–66.

Lawson, P. R., B. Baker, C. G. Schmitt, and T. Jensen, 2001: An overview of microphysical properties of Arctic clouds observed in May and June 1998 during FIRE ACE. *J. Geophys. Res.*, **106** (D14), 14 989–15 014.

Liou, K. N., and Y. Takano, 1994: Light scattered by non-spherical particles: Remote sensing and climate implications. *Atmos. Res.*, **31,** 271–298.

List, R., and R. S. Schemenauer, 1971: Free-fall behavior of planar snow crystals, conical graupel, and small hail. *J. Atmos. Sci.*, **28,** 110–115.

Magono, C., and C. Lee, 1966: Meteorological classification of natural snow crystals. *J. Fac. Sci. Hokkaido Univ.*, **2,** 321–335.

Mazin, I. P., A. V. Korolev, A. Heymsfield, G. A. Isaac, and S. G. Cober, 2001: Thermodynamics of icing cylinder for measurements of liquid water content in supercooled clouds. *J. Atmos. Oceanic Technol.*, **18,** 543–558.

Nakaya, U., 1954: *Snow Crystals, Natural and Artificial*. Harvard University Press, 510 pp.

Ono, A., 1969: The shape and riming properties of ice crystals in natural clouds. *J. Atmos. Sci.*, **26,** 138–147.

Rottner, D., and G. Vali, 1974: Snow crystal habit at small excesses of vapor density over ice saturation. *J. Atmos. Sci.*, **31,** 560–569.

Stith, J. L., J. E. Dye, A. Bansemer, A. J. Heymsfield, C. A. Grainger, W. A. Petersen, and R. Cifelli, 2002: Microphysical observations of tropical clouds. *J. Appl. Meteor.*, **41,** 97–117.

Strapp, J. W., P. Chow, M. Moltby, A. D. Beezer, A. V. Korolev, I. Stronberg, and J. Hallett, 1999: Cloud microphysical measurements in thunderstorm outflow regions during Allied/BAE 1997 flight trials. *Proc. AIAA 37th Aerospace Sciences Meeting and Exhibit*, Reno, NV, AIAA 99-0498.

Zhang, Y., A. Macke, and F. Albers, 1999: Effect of crystal size spectrum and crystal shape on stratiform cirrus radiative forcing. *Atmos. Res.*, **52,** 59–75.